JOURNAL OF COMPUTATIONAL PHYSICS 78, 288–304 (1988)

Spline-Collocation with Adaptive Mesh Grading for Solving the Stochastic Collection Equation

D. EYRE AND C. J. WRIGHT

National Research Institute for Mathematical Sciences of the CSIR, P. O. Box 395, Pretoria 0001, Republic of South Africa and
**Department of Computational and Applied Mathematics and Centre for Nonlinear Studies, University of the Witwatersrand, WITS 2050, Republic of South Africa*

AND

G. REUTER†

Atmospheric Sciences Division, National Physical Research Laboratory of the CSIR, P.O. Box 395, Pretoria 0001, Republic of South Africa

Received June 17, 1987; revised November 18, 1987

The method of collocation using cubic B-splines and an adaptive mesh is applied to the solution of the partial integro-differential equation that describes the continuous mass spectrum of particles undergoing stochastic collection growth. Temporal discretization and a number of explicit and implicit linear multistep methods are employed to solve the system of ordinary differential equations. The numerical method is tested by solving model problems that describe the coalescence of particles for both single and double initial distributions. It is found that accurate solutions can be obtained using a small number of B-splines, and that adaptive mesh grading improves the accuracy of the solutions without needing additional nodal points.

1. INTRODUCTION

The time evolution of a continuous spectrum of particles undergoing stochastic collection growth is described by the stochastic collection equation that has the form

$$\frac{\partial}{\partial t} N(m, t) = \int_0^{m/2} N(M, t)\, N(m-M, t)\, K(M, m-M)\, dM - N(m, t) \int_0^{\infty} N(M, t)\, K(M, m)\, dM. \tag{1.1}$$

* Permanent address.

† Present address: Department of Meteorology, McGill University, 805 Sherbroke Street West, Montreal, Quebec H3A 2K6, Canada.

0021-9991/88 $3.00

Here $N(m, t)\,dm$ is the average number of particles per unit volume of space with masses between m and $m + dm$ at time t, and $K(M, m)$ is the collection kernel that is a symmetric function of its two arguments and has the units of volume per time. The function K represents the geometry and dynamics of the collision mechanism. The terms on the right-hand side of Eq. (1.1) can be understood as follows: The first term represents the rate of increase of particles by collection of smaller particles. The upper limit of $m/2$ prevents overcounting. The second term represents the loss of particles due to collection with particles of all masses. Equation (1.1) is often expressed in volume (rather than mass) coordinates. Both mass and volume are conserved quantities.

Equation (1.1) describes a number of phenomena in which mobile particles collide with each other and fuse. Examples of such coalescence processes are aerosol agglomeration [1], coalescence of voids and bubbles in irradiated materials, and the growth of inclusion in castings [2]. Our interest in the stochastic collection equation arises from its applications to examining the formation of raindrops via coalescence of cloud droplets. For the last three decades, the "classical" problem of cloud microphysics has been to explain the rapid development of rain [3]. An accurate and economical scheme to solve the stochastic collection equation is mandatory to enable progress to be made in this field.

For studying rain formation in convective clouds, (1.1) is to be embedded in the dynamic and thermodynamic equations that govern the time-dependent three-dimensional airflow of the cloud convection. This means that (1.1) has to be solved at each time step for each grid point of the numerical cumulus model. For three-dimensional cloud models this results in very high computational demands. It is thus mandatory to represent the spectrum of cloud and rain particle sizes with as few classes as possible. To maximize the information on the structure of the size spectrum, the size classes (or nodal points of the numerical scheme) should be chosen in an optimal way. Furthermore, the choice of size classes should be updated at regular intervals to remain close to the optimal partitioning. This paper deals with numerical schemes that have this desired feature of adaptive mesh grading.

The theoretical justification of Eq. (1.1) has been investigated by a number of authors [4–7]. A detailed discussion of the stochastic completeness of Eq. (1.1) is given by Gillespie [5]. The stochastically complete equation has been solved using Monte Carlo simulation techniques. Recent calculations [7] show that discrepancies may exist between the solution of Eq. (1.1) and the true stochastic averages.

Exact solutions of Eq. (1.1) have been obtained in a few exceptional cases [8]. These analytic solutions provide a useful test of the accuracy of approximate numerical solutions [9–13]. The general problem, however, can be solved only by approximate numerical methods [14–15]. A complete understanding of stochastic coalescence in realistic situations is therefore limited by the accuracy of the numerical solutions.

The first step in solving Eq. (1.1) is to discretize the mass variables. Our approach is to map Eq. (1.1) onto a finite domain and then to approximate the

solution function by a linear combination of trial functions. The difficulty with this approach is that the efficiency of the method will depend on finding a suitable trial space. A number of the methods used in practice employ piecewise polynomials for discretizing the mass. For example, the successful approach used by Bleck [10] employs piecewise constant functions. The result of using this approximation is that the approximate solution is discontinuous at the nodes. Another approach [13], which is the one we shall use, is to choose cubic splines. The cubic spline approximation is smooth (C^2 continuity at the nodes) and yields an approximate equation with better convergence properties than the method based on piecewise constant functions.

The choice of nodal points is expected to be important. In particular, a good choice of nodal points will reduce the number of trial functions that are needed for an accurate solution of Eq. (1.1). In all of the previous numerical approaches the nodes are fixed and do not vary. In our approach, however, the nodes are allowed to move. Since the structure of the solution function may vary considerably with time, we have used adaptive mesh grading to optimize the position of the nodal points. This optimization is performed by equidistributing the nodal points with respect to the arc lengths of the approximate solution function [16].

A collocation method reduces the problem of solving Eq. (1.1) to that of solving a system of first-order ordinary differential equations for the expansion coefficients. Several numerical schemes are employed to evaluate these coefficients: the classical one-step θ-method, which includes, as special cases, an explicit scheme, the Crank–Nicolson scheme, and a fully implicit scheme. We also implement multistep methods such as the Adams predictor-corrector schemes and Gear's method for stiff systems.

A conserved quantity arising from Eq. (1.1) is the moment integral

$$\int_0^\infty N(m, t)\, m dm = N_0\, m_0, \tag{1.2}$$

where m_0 is the initial average mass of the particles and N_0 is the initial number of particles per unit volume.

An important feature of the present method is that it does not explicitly use the conserved quantity (1.2). We can therefore use this integral as an independent test of the accuracy of our numerical solution. In cloud physics (1.2) is referred to as the liquid water content (LWC).

Section 2 describes the approximation method. Section 3 gives our numerical results, including a comparison of results using non-adaptive and adaptive mesh grading. Comparisons are made between numerical and analytic solutions for two types of kernels, one being the sum of its arguments and the other a constant. The equation with double initial distribution is also solved. Our conclusions are given in Section 4.

2. The Approximation Method

This section describes our numerical method for solving Eq. (1.1). The three basic components of this method are (i) cubic spline approximation, (ii) adaptive mesh grading, and (iii) linear multistep methods. The adaptive mesh grading is optional and may be "switched off" if necessary.

A major problem to be overcome when dealing with Eq. (1.1) for the liquid drop problem is that the mass spectrum of droplets can range over many orders of magnitude. We shall take this variation into account by suitably transforming the mass coordinates. It is convenient to map the mass coordinates m, $M \in [0, \infty)$ onto dimensionless variables q, $Q \in [-1, 1]$. For this purpose we use the transformation

$$m = \zeta\left(\frac{1+q}{1-q}\right), \qquad M = \zeta\left(\frac{1+Q}{1-Q}\right), \tag{2.1}$$

where ζ is a "free" mass parameter. The transformed equation (1.1) becomes

$$\frac{\partial}{\partial t} v(q, t) = 2\zeta \int_{-1}^{q(m/2)} v(\tilde{q}, t)\, v(Q, t)\, k(Q, \tilde{q}) \frac{dQ}{(1-Q)^2} - 2\zeta v(q, t) \int_{-1}^{1} v(Q, t)\, k(Q, q) \frac{dQ}{(1-Q)^2}, \tag{2.2}$$

where

$$q\left(\frac{m}{2}\right) = \left(\frac{m-2\zeta}{m+2\zeta}\right) \tag{2.3}$$

and

$$\tilde{q}(q, Q) = \frac{2(q-Q) - (1-q)(1-Q)}{2(q-Q) + (1-q)(1-Q)} \tag{2.4}$$

is the transformed mass difference $m - M$. The mapping (2.1) introduces a singularity at $Q = 1$ in the kernel of Eq. (2.2). It should be noted, however, that the second integral in Eq. (2.2) is not singular if the integrand decreases sufficiently rapidly, for example, as an exponential.

We now consider the problem of mass discretization. We seek an approximation to the (unknown) solution $v(q, t)$ of Eq. (2.2) which satisfies some interpolation property. To this end we choose as our approximating functions the finite linear space of cubic splines with a given set of nodal points [17]. To be specific, let π_n be a partition of the interval $[-1, 1]$ defined by the nodal points $-1 = s_{n,1} < s_{n,2} < \cdots < s_{n,n} = 1$. On this partition, together with the extended knots $s_{n,-2} \leqslant s_{n,-1} \leqslant s_{n,0} \leqslant s_{n,1}$ and $s_{n,n} \leqslant s_{n,n+1} \leqslant s_{n,n+2} \leqslant s_{n,n+3}$, we can construct cubic B-splines [18, 19]. We denote the B-splines by $\{B_{n,i}\}_{i=0}^{n+1}$, where each function $B_{n,i}$ is non-zero over an interval $(s_{n,i-2}, s_{n,i+2})$. The cubic B-splines form a basis for a

linear space of cubic splines on π_n with C^2 continuity over $[-1, 1]$. Using this linear space, we can now approximate the function $v(q, t)$ by the linear combination

$$\sum_{i=0}^{n+1} f_{n,i}(t)\, B_{n,i}(q). \tag{2.5}$$

We now discuss the adaptive mesh grading procedure. The end nodes and the three additional nodes on either end of the interval $[-1, 1]$ remain fixed. The position of these additional nodes has no effect on the spline approximation in the interval $[-1, 1]$. Since the procedure is applied at some fixed time, we temporarily suppress the variable t. Let $u(q)$ be the cubic B-spline approximation (2.5) on the partition π_n, and let

$$\eta_i = \int_{s_{n,i-1}}^{s_{n,i}} \left[1 + \left(\frac{du}{dq}\right)^2\right]^{1/2} dq, \qquad i = 2, \ldots, n, \tag{2.6}$$

be the arc lengths of $u(q)$ over the subintervals $I = [s_{n,i-1}, s_{n,i}]$.

Our approach to adaptive mesh grading is to equidistribute the nodal points with respect to the arc lengths. Extreme values are damped by introducing a weighted means quantity for the interior subintervals

$$\beta_i = \sum_{j=0}^{2l} \rho_j \eta_{i+j-l}, \qquad i = l+2, \ldots, n-l. \tag{2.7}$$

Similar but one-sided means are used for the boundary subintervals. The value of l is chosen to fix the width of the interval of influence. For our numerical examples we have chosen $l = 1$, $\rho_0 = \rho_2 = \frac{1}{4}$ and $\rho_1 = \frac{1}{2}$.

The measure of arc length is obtained by summing β. After applying inverse linear interpolation to equidistribute the measure (2.6) with respect to the nodal points, we arrive at a new partition, $\hat{\pi}_n$.

The above procedure can be applied iteratively until convergence of the mesh is achieved. We employ two criteria for convergence. The first criterion is based on an equidistribution of the quantities $\{\beta_i\}$ so that

$$\sigma = \left[\sum_{i=2}^{n} (\beta_i - \bar{\beta})^2\right]^{1/2} \Big/ (n-1) \tag{2.8}$$

is less than some specified tolerance. Here $\bar{\beta}$ is the average value of $\{\beta_i\}$. The second criterion is based on how far the nodal points have moved from their previous position. Let $\{s_{n,i}\}$ and $\{\hat{s}_{n,i}\}$ be the old and new points, respectively. If h is the average separation of points, then our second criterion for convergence can be written as

$$|\hat{s}_{n,i} - s_{n,i}| < \varepsilon h, \qquad i = 1, \ldots, n. \tag{2.9}$$

where ε is a specified tolerance. If either of the above two conditions are satisfied then the set of points $\{\hat{s}_{n,i}\}$ is assumed to have converged. The tolerance values must be found by trial and error and depend on the problem which is being solved.

We now return to the approximate solution (2.5). From Eqs. (2.2) and (2.5) the time evolution equation becomes

$$\frac{\partial}{\partial t}\sum_{i=0}^{n+1} f_{n,i}(t)\, B_{n,i}(q) = \sum_{j=0}^{n+1}\sum_{k=0}^{n+1} f_{n,j}(t) f_{n,k}(t)\, c_{jk}(q), \tag{2.10}$$

where $c_{jk}(q)$ is defined by moment integrals

$$c_{jk}(q) = 2\zeta \int_{-1}^{q(m/2)} B_{n,j}(\tilde{q})\, B_{n,k}(Q)\, k(Q,\tilde{q}) \frac{dQ}{(1-Q)^2} - 2\zeta B_{n,j}(q) \int_{1}^{1} B_{n,k}(Q)\, k(Q,q) \frac{dQ}{(1-Q)^2}. \tag{2.11}$$

On introducing $(n+2)$ collocation points $\{r_{n,l}\}_{l=0}^{n+1} \in [-1, 1]$ and collocating, we obtain the system of first-order ordinary differential equations

$$\sum_{i=0}^{n+1} B_{n,i}(r_{n,l})\dot{f}_{n,i}(t) = \mathbf{f}^{\mathrm{T}}\mathbf{C}_l\mathbf{f}, \qquad l = 0, 1, ..., n+1. \tag{2.12}$$

Here $\mathbf{f}^{\mathrm{T}} := [f_{n,0}(t), f_{n,1}(t), ..., f_{n,n+1}(t)]$ is an $(n+2)$ vector, and $\mathbf{C}_l := [c_{jk}(r_{n,l})]$ is an $(n+2)\times(n+2)$ matrix. Further, defining the $(n+2)\times(n+2)$ matrix $\mathbf{\Phi} := [B_{n,i}(r_{n,l})]$, we may rewrite Eq. (2.12) as

$$\mathbf{\Phi}\dot{\mathbf{f}} = \begin{bmatrix} \mathbf{f}^{\mathrm{T}} & \mathbf{C}_0 & \mathbf{f} \\ \mathbf{f}^{\mathrm{T}} & \mathbf{C}_1 & \mathbf{f} \\ & \vdots & \\ \mathbf{f}^{\mathrm{T}} & \mathbf{C}_{n+1} & \mathbf{f} \end{bmatrix} = \mathbf{g}. \tag{2.13}$$

To ensure that the matrix $\mathbf{\Phi}$ is invertible, the choice of collocation points $\{t_{n,l}\}_{l=0}^{n+1}$ is restricted by the Schoenberg–Whitney theorem [17, p. 200, Theorem XIII.1], which requires that

$$s_{n,i-2} < r_{n,i} < s_{n,i+2}, \qquad i = 0, 1, ..., n+1. \tag{2.14}$$

The following choice of collocation points is used:

$$r_{n,0} = s_{n,1}; \qquad r_{n,1} = (s_{n,1} + s_{n,2})/2;$$
$$r_{n,i} = s_{n,i}, \qquad i = 2, ..., n-1;$$
$$r_{n,n} = (s_{n,n-1} + s_{n,n})/2; \qquad r_{n,n} = s_{n,n}. \tag{2.15}$$

We now turn to numerical schemes for solving the system (2.13):

I. *Classical One-Step θ Method*

Let Δt denote the current time step, $\mathbf{f}_t = \mathbf{f}(t)$, and $\mathbf{f}_{t+1} = \mathbf{f}(t+\Delta t)$. The θ-method for (2.15) is defined by the finite difference equation

$$\mathbf{\Phi f}_{t+1} - \theta \Delta t \mathbf{g}_{t+1} = \mathbf{\Phi f}_t + (1-\theta)\,\Delta t \mathbf{g}_t. \tag{2.16}$$

We investigate three frequently used cases:

(i) $\theta = 0$, which is the usual explicit scheme, namely

$$\mathbf{\Phi f}_{t+1} = \mathbf{\Phi f}_t + \Delta t \mathbf{g}_t; \tag{2.17}$$

(ii) $\theta = \frac{1}{2}$, which is the Crank–Nicolson method, namely

$$\mathbf{\Phi f}_{t+1} - \tfrac{1}{2}\Delta t \mathbf{g}_{t+1} = \mathbf{\Phi f}_t + \tfrac{1}{2}\Delta t \mathbf{g}_t; \tag{2.18}$$

(iii) $\theta = 1$, which is the fully implicit scheme, namely

$$\mathbf{\Phi f}_{t+1} - \Delta t \mathbf{g}_{t+1} = \mathbf{\Phi} \boldsymbol{f}_t. \tag{2.19}$$

Notice that both (2.18) and (2.19) are non-linear in $\mathbf{f}_{t+1}$. We discuss both schemes together in Eq. (2.16), where we use the following algorithm: We obtain an initial estimate from (2.17), that is,

$$\mathbf{\Phi f}_{t+1}^{(0)} = \mathbf{\Phi f}_t + \Delta t \mathbf{g}, \tag{2.20}$$

and iterate

$$\mathbf{\Phi f}_{t+1}^{(j+1)} = \mathbf{\Phi f}_t + (1-\theta)\,\Delta t \mathbf{g}_t + \theta \Delta t \mathbf{g}_{t+1}^{(j)}. \tag{2.21}$$

II. *Higher Order Multistep Methods*

The general multistep method of stepnumber k is defined by the formula

$$\sum_{j=0}^{k} \mathbf{\Phi} \boldsymbol{f}_{i+j} \alpha_j = \Delta t \sum_{j=0}^{k} \mathbf{g}_{i+j} \beta_j, \tag{2.22}$$

where α_j and β_j are constants.

A standard IMSL subroutine DGEAR was used in this case. The package makes use of Adams predictor-corrector schemes, as well as Gear's method for stiff systems [20].

For some of these methods the right-hand side of the equation

$$\dot{\mathbf{f}} = \mathbf{\Phi}^{-1}\mathbf{g} \tag{2.23}$$

must be computed or estimated. Let $\mathbf{\Phi}^{-1} = [\mu_{ij}]$. The required Jacobian is

$$J_{ij} = \sum_{k=0}^{n+1} [d_{kj}(r_{n,i}) + d_{jk}(r_{n,i})] f_{n,k}, \tag{2.24}$$

where $\mathbf{D}_i := [d_{kj}(r_{n,i})]$ is defined by

$$\mathbf{D}_k = \sum_{l=0}^{n+1} \mu_{kl} \mathbf{C}_l. \tag{2.25}$$

3. Numerical Examples

In the formulation of numerical procedures to test the validity of the approximation method we have paid particular attention to the numerically stable methods used in the sub-procedures.

The cubic B-splines were evaluated using the iterative technique of Cox [18]. This procedure is both fast and accurate. The next step is to evaluate the moment integrals $c_{jk}(r_{n,l})$ in Eq. (2.11). These integrals were evaluated using IMSL subroutine DCADRE. The actual moments were calculated over intervals $[s_i, s_{i+1})$ and summed.

In the case of adaptive mesh grading the initial condition is first approximated by a cubic spline on a uniformly spaced mesh. The coefficients in Eq. (2.5) are scaled to $\hat{f}_{n,i}$, where

$$\max_{q \in [-1,1]} \left| \sum_{i=0}^{n+1} \hat{f}_{n,i}(t)\, B_{n,i}(q) \right| = 1. \tag{3.1}$$

The adaptive mesh grading procedure described in Section 2 is performed on the initial condition and is repeated after a fixed number of time steps.

To test our method for solving the stochastic collection equation (1.1) we first compare numerical results against analytic solutions [8]. For the initial condition we take

$$N(m, 0) = \frac{N_0}{m_0} \frac{(\gamma+1)^{\gamma+1}}{\Gamma(\gamma+1)} \left(\frac{m}{m_0}\right)^{\gamma} \exp\{-m/m_0)(\gamma+1)\}, \tag{3.2}$$

where $\gamma \geqslant 0$.

We shall consider two simple cases for the collection kernel:

I. *Golovin* [21] *kernel:*

$$K(M, m) = b(m + M). \tag{3.3}$$

Scott [8] gives the solution for $\gamma = 0$ as

$$N(m, t) = \frac{N_0}{m} \frac{(1-\tau)}{\sqrt{\tau}} \exp\left[-\left(\frac{m}{m_0}\right)(\tau+1) \right] I_1\left[2\left(\frac{m}{m_0}\right)\sqrt{\tau} \right], \tag{3.4}$$

where $\tau = 1 - e^{-T}$, $T = bm_0 N_0 t$ is the dimensionless time, and I_1 is the modified Bessel function of the first kind of order one:

$$I_1(x) = \sum_{l=0}^{\infty} \frac{(x/2)^{2l+1}}{l!(l+1)!}. \tag{3.5}$$

II. *Constant kernel:*

$$K(M, m) = c. \tag{3.6}$$

For this example Scott [8] gives the solution for $\gamma = 0$ as

$$N(m, t) = \frac{N_0}{m_0} \frac{4}{(T+2)^2} \exp\left[-\left(\frac{m}{m_0}\right) \frac{2}{(T+2)} \right], \tag{3.7}$$

and for $\gamma = 1$ as

$$N(m, t) = 8 \frac{N_0}{m_0} \exp\left\{ -2(m/m_0) \right\} \frac{\sinh\{(2m/m_0)[T/(T+2)]^{1/2}}{T^{1/2}(T+2)^{3/2}}, \tag{3.8}$$

where $T = cN_0 t$ is the dimensionless time.

Numerical examples are chosen to describe the cloud water droplet problem approximately. For the initial value we take $N_0 = 2.3874(2)$ cm^{-3} and $m_0 = 4.1887(-3)$ μg. (The mass m_0 corresponds to a mean drop radius of about 10 μm, while the liquid water content (LWC) is $N_0 m_0 = 1.0$ μg cm^{-3}.) Parameters for the collection kernels I and II are chosen to be $b = 1.53(-3)$ cm^3 μg^{-1} s^{-1} and $c = 1.8(-4)$ cm^3 s^{-1}, respectively.

Numerical results are obtained for four examples, which represent some of our typical results for the method. For convenience we have tabulated the examples in Table I. We note that Eq. (1.1) is defined on an infinite mass domain, and that mapping (2.1) onto a finite domain introduces a singularity. The method used to deal with this singularity is to truncate the domain so that $q, Q \in [-1, q_c]$. We remark that when the exact solution is known then it is possible to estimate the

TABLE I

Tabulation of the Numerical Examples

Example	Collection kernel	Initial condition
1	$b(m+M)$	$\gamma = 0$
2	c	$\gamma = 0$
3	c	$\gamma = 1$
4	$b(m+M)$	Double exponential ($\gamma = 0$)

error introduced by the domain truncation [13]. In all of the numerical examples the mapping parameter ζ is chosen so that the initial condition $v(q, 0)$ is not concentrated in a small region of the interval $[-1, 1]$. The cutoff parameter q_c is chosen so that it does not affect the computed results significantly. In order to satisfy these requirements we have chosen the mapping and cutoff parameters to be $\zeta = 0.03$ μg and $q_c = 0.9$, respectively.

In the case of the θ-method we have used a step length of $\Delta t = 5s$, but for Gear's method a variable step length is used by subroutine DGEAR. In practice, we find very little difference between the results obtained with different linear multistep methods. We therefore make no distinction between these methods when presenting our numerical results.

The accuracy of the approximate solution $v_A(q, t)$ is measured in two ways: The first is to compute the approximate LWC by evaluating the truncated integral

$$(\mathrm{LWC})_A = \int_{-1}^{q_c} \tilde{v}_A(q, t)\, dq, \tag{3.9}$$

where

$$\tilde{v}_A(q, t) = 2\zeta^2 \frac{(1+q)}{(1-q)^3} v_A(q, t). \tag{3.10}$$

A further measure of the approximate solution is provided by the L_∞-norm of the relative error

$$\|e\|_\infty = \max_{q \in [-1, 1]} \left| \frac{v_A(q, t) - v(q, t)}{1 + v(q, t)} \right|. \tag{3.11}$$

Note that while it is always possible to evaluate the integral (3.9), it is only possible to calculate the relative norm if the exact solution $v(q, t)$ is known.

We first consider the case of initial condition (3.2) with $\gamma = 0$. Tables II and III show results for the Golovin and constant kernels, respectively. The results are obtained with $n = 12$ nodes. In both examples a definite improvement in the accuracy of the approximate solution is achieved by using the adaptive mesh grading procedure. Figures 1 and 2 show the profile of the approximate solutions $\tilde{v}_A(q, t)$ for the Golovin and constant kernels, respectively. In the case of the Golovin kernel there is no discernible difference between the approximate and the exact solutions. However, the profile for the constant kernel does deviate from the exact solution over a period of 10 min and at the large mass end of the spectrum. This discrepancy disappears when we use a finer mesh with $n = 22$ nodes. Qualitatively, the Golovin kernel tends to spread the mass spectrum, whereas the constant kernel tends to shift the mass spectrum to the larger mass droplets.

We next consider the initial condition (3.2) with $\gamma = 1$. (This function exhibits more structure than the $\gamma = 0$ case.) Table IV shows the result for the constant kernel using $n = 12$ nodes and $\Delta t = 5s$. Figure 3 shows the profile of the approximate

TABLE II

Results for the Golovin Kernel (Example 1) after 1 min Intervals Using $n = 12$ Nodes

t	No regrid		Regrid	
	$(LWC)_A$	$\|e\|_\infty$	$(LWC)_A$	$\|e\|_\infty$
0	0.999	1(−6)	0.998	8(−7)
1	1.008	3(−2)	1.000	1(−1)
2	1.017	5(−2)	0.999	1(−1)
3	1.025	1(−1)	0.999	8(−2)
4	1.035	1(−1)	1.004	1(−1)
5	1.047	2(−1)	1.013	1(−1)
6	1.060	2(−1)	1.018	8(−2)
7	1.071	3(−1)	1.017	9(−2)
8	1.080	3(−1)	1.013	9(−2)
9	1.087	3(−1)	1.007	6(−2)
10	1.093	2(−1)	1.004	3(−2)

Note. The exact liquid water content (LWC) is 1.0 $\mu g\ cm^{-3}$.

TABLE III

Results for the Constant Kernel and Initial Condition with $\gamma = 0$ (Example 2) Using the Parameters of Table I

t	No regrid		Regrid	
	$(LWC)_A$	$\|e\|_\infty$	$(LWC)_A$	$\|e\|_\infty$
0	0.999	1(−6)	0.998	8(−7)
1	1.041	1(−1)	1.009	5(−2)
2	1.047	1(−1)	1.009	1(−1)
3	1.063	2(−1)	1.038	7(−2)
4	1.079	1(−1)	1.053	4(−2)
5	1.080	2(−1)	1.047	7(−2)
6	1.071	2(−1)	1.030	8(−2)
7	1.059	2(−1)	1.012	7(−2)
8	1.049	2(−1)	0.999	5(−2)
9	1.042	1(−1)	0.991	5(−2)
10	1.039	2(−1)	0.990	4(−2)

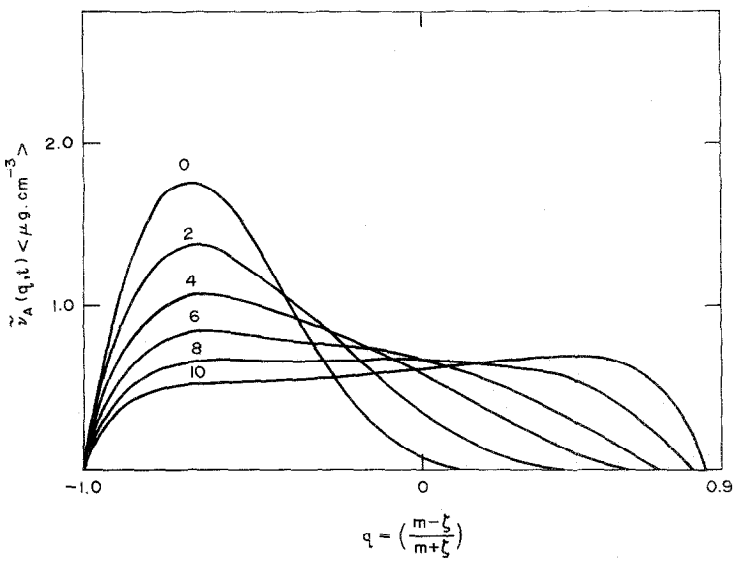

FIG. 1. Profile of the approximate solution $\tilde{v}_A(q, t)$ for the Golovin kernel (Example 1) using $n = 12$ nodes and $\Delta t = 5s$. Each curve is labeled by the time in minutes.

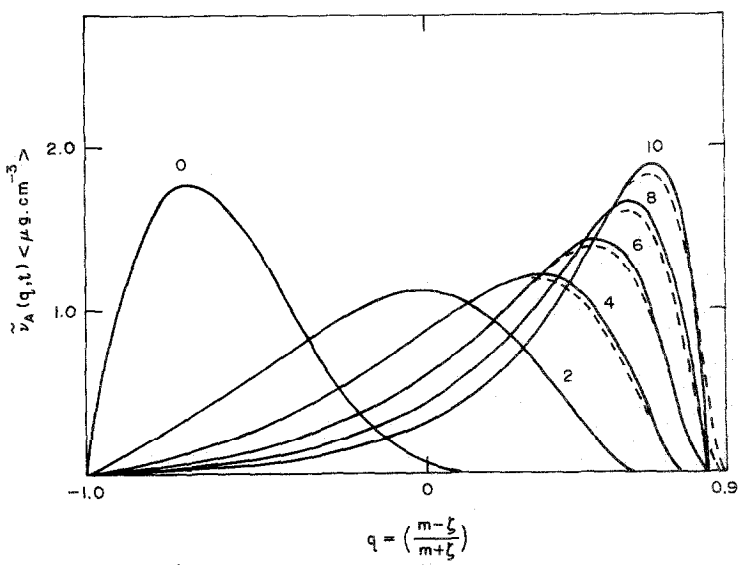

FIG. 2. Same as Fig. 1 for the constant kernel and initial condition $\gamma = 0$ (Example 2). The exact (broken) and approximate (solid) curves are shown.

TABLE IV

Results for Constant Kernel and Initial Condition with $\gamma = 1$ (Example 3) Using the Parameters of Table I; no regridding

t	$(\mathrm{LWC})_A$	$\|e\|_\infty$
0	1.001	7(−3)
1	1.002	3(−2)
2	0.995	4(−2)
3	1.001	9(−2)
4	1.014	6(−2)
5	1.018	3(−2)
6	1.012	5(−2)
7	1.002	5(−2)
8	0.991	5(−2)
9	0.983	2(−2)
10	0.978	1(−2)

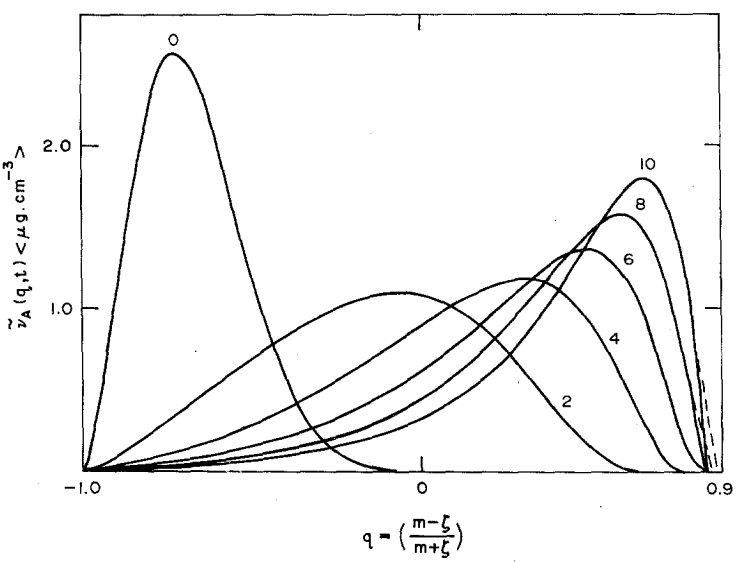

FIG. 3. Same as Fig. 1 for the constant kernel and initial condition $\gamma = 1$ (Example 3). The exact (broken) and approximate (solid) curves are shown.

solution $\tilde{v}_A(q, t)$. For this example it as found that adaptive mesh grading does not improve the accuracy of the approximate solution. Nevertheless, sufficient accuracy was achieved without regridding.

A detailed investigation of the reasons for the failure of the adaptive mesh grading procedure for example 3 uncovered the following: The spline interpolation can oscillate in regions between collocation points. If no regridding is performed, then only the original collocation points are used in the time stepping and the oscillations do not contribute to the error. If, on the other hand, one attempts to regrid from the spline interpolant, then the oscillations will contribute to the error in subsequent time steps. The result is that the error due to the oscillations will grow with time, and a poor approximation results.

We now investigate a problem that does not have an analytic solution. We consider the Golovin kernel. For the initial condition we take a double distribution [12]

$$N(m, 0) = x(N_0/m_0)\exp(-m/m_0) + (1-x)\ (N_1/m_1)\exp(-m/m_1). \quad (3.12)$$

Here $m_1 = 8m_0$, and $x = 0.8$, where x is the fraction of the LWC contained in the first term. (The total LWC is $N_0 m_0 = N_1 m_1 = 1.0\ \mu g\ cm^{-3}$.) Figure 4 shows the profile of the approximate solution using $n = 32$ nodes. The double distribution of the initial condition can be seen clearly. As time progresses, the bump on the left-hand side disappears, whereas the bump on the right-hand side grows with a peak moving to the larger mass end of the spectrum. Table V shows results for the $(LWC)_A$ using $n = 32$ and $n = 14$ nodes over a period of 10 min. The error for $n = 32$ is less than 1%, while the error for $n = 14$ is less than 4%. The result of regridding using $n = 14$ nodes is shown in the last column. Here we see that the effect of regridding is to improve the accuracy of the approximation significantly for

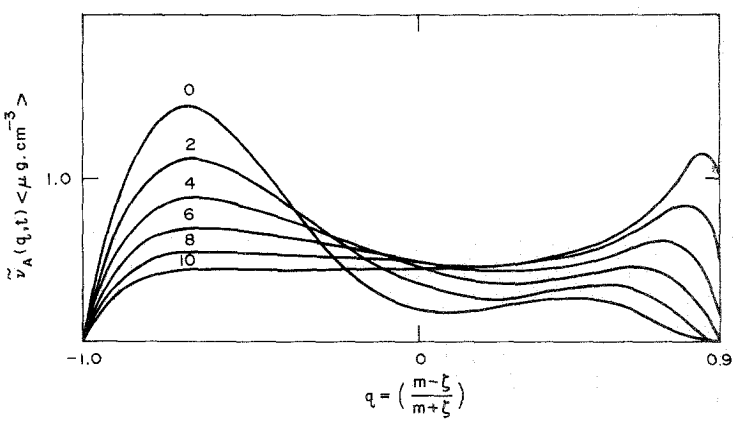

FIG. 4. Profile of the approximate solution $\tilde{v}_A(q, t)$ for the Golovin kernel and initial double distribution (Example 4) using $n = 32$ nodes.

TABLE V

Results for Golovin Kernel and Initial Double Distribution (Example 4)

t	No regrid		Regrid
	$n=32$	$n=14$	$n=14$
0	1.000	1.002	1.003
1	1.001	1.006	1.002
2	1.003	1.012	1.001
3	1.005	1.018	1.000
4	1.006	1.024	1.000
5	1.006	1.024	1.000
6	1.007	1.029	1.000
7	1.007	1.032	1.000
8	1.005	1.034	0.998
9	1.000	1.033	0.994
10	0.993	1.027	0.986

Note. The $(LWC)_A$ is calculated using $n=32$ and $n=14$ nodes.

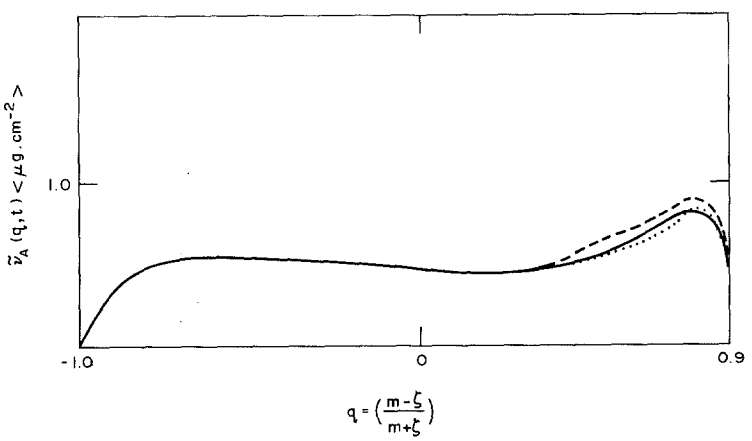

FIG. 5. Profile of the approximate solution $\tilde{v}_A(q, t)$ for the Golovin kernel and initial double distribution (Example 4) after 8 min showing the $n=32$ no regridding (solid) curve, the $n=14$ no regridding (broken) curve, and the $n=14$ with regridding (dotted) curve.

much of the time interval. Figure 5 shows the profile after 8 min for the above three cases. Here we see that the effect of regridding is to improve the profile, particularly at the longer mass end of the spectrum. The truncation of the interval at $q_c = 0.9$ introduces an error of less than 1% in the LWC, as can be seen from Table V.

4. Summary

A numerical scheme for solving the stochastic collection equation has been used to solve a number of model problems that approximately describe water droplet coalescence. For the problems we have considered there is little or no difference between the different linear multistep methods. The subroutine DGEAR is more sophisticated than the simple one-step θ-method but requires more computer time. DGEAR is therefore used only to check the accuracy of results using the θ-method. The major source of error is the coarse mesh that is used for the spline interpolation. Since the mass spectrum extends over many orders of magnitude, an appropriate mapping of the infinite mass domain is required. The choice of mapping parameter ζ is critical for the success of the method. In a global sense this mapping can be regarded as a method for positioning the nodal points. A further adjustment of the mesh can be obtained by equidistributing these points with respect to the measure (2.6). The numerical method permits an independent check of the approximate solution simply by calculating the LWC, which is a conserved quantity for the exact solution.

This study has shown that the stochastic collection equation can be solved accurately using only a small number of B-splines, provided that the nodal points are chosen optimally and that the grid arrangement is adapted as the size spectrum evolves.

Furthermore, some examples have shown that adaptive mesh grading can improve the accuracy of the numerical solution significantly without using additional nodal points. The numerical scheme presented seems attractive for use in the three-dimensional numerical models of clouds in which coalescence of droplets is an important mechanism of rain formation.

References

1. H. R. Pruppacher and J. D. Klett, *Microphysics of Clouds and Precipitation* (Reidel, Dordrecht/Boston/London, 1978).
2. J. W. Hilgers, R. J. Spahn, and T. H. Courtney, *Math. Modelling* **6**, 463 (1985).
3. I. R. Paluch and C. A. Knight, *J. Atmos. Sci.* **43**, 1994 (1986).
4. S. Twomey, *J. Atmos. Sci.* **23**, 405 (1966).
5. D. T. Gillespie, *J. Atmos. Sci.* **29**, 1496 (1972).
6. D. T. Gillespie, *J. Atmos. Sci.* **32**, 600 (1975).
7. I. A. Valioulis and E. J. List, *J. Atmos. Sci.* **41**, 2516 (1984).
8. W. T. Scott, *J. Atmos. Sci.* **25**, 54 (1968).

9. E. X. BERRY, *J. Atmos. Sci.* **75**, 688 (1967).
10. R. BLECK, *J. Geophys. Res.* **75**, 5165 (1970).
11. L. D. NELSON, *J. Atmos. Sci.* **28**, 752 (1971).
12. E. X. BERRY AND R. L. REINHARDT, *J. Atmos. Sci.* **31**, 1814 (1974); **31**, 1825 (1974).
13. F. GELBARD AND J. H. SEINFELD, *J. Comput. Phys.* **28**, 357 (1978).
14. P. S. BROWN, JR., *J. Comput. Phys.* **58**, 417 (1985).
15. P. S. BROWN, JR., *J. Climate Appl. Meteorol.* **25**, 313 (1986).
16. W. HAASE, K. MISEGADES, AND M. NAAR, *Int. J. for Num. Meth. in Fluids* **5**, 515 (1985).
17. C. DE BOOR, *A Practical Guide to Splines* (Springer-Verlag, New York/Heidelberg/Berlin, 1978).
18. M. G. COX, *J. Inst. Math. Appl.* **10**, 134 (1972).
19. C. DE BOOR, *J. Approx. Theory* **6**, 50 (1972).
20. C. W. GEAR, *Numerical Initial Value Problems in Ordinary Differential Equations* (Prentice–Hall, Englewood Cliffs, NJ, 1971).
21. A. M. GOLOVIN, *Soviet Phys. Dokl.* **8**, 191 (1963).